PCCP

Electrochemical reactions of lithium-sulfur batteries: an analytical study using the organic conversion technique

Journal:	*Physical Chemistry Chemical Physics*
Manuscript ID:	CP-ART-03-2014-000958
Article Type:	Paper
Date Submitted by the Author:	06-Mar-2014

Complete List of Authors:	Kawase, Ayako; Daihatsu Motor Co.,Ltd., R&D Division Shirai, Shoichi; Toyota Central R&D Laboratories, Inc., Inorganic Materials Division Yamoto, Yoshinari; Kansai University, Department of Applied Chemistry Arakawa, Ryuichi; Kansai University, Department of Applied Chemistry Takata, Toshikazu; Tokyo Institute of Technology, Department of Organic and Polymeric Materials

Journal Name

RSCPublishing

ARTICLE

Electrochemical reactions of lithium-sulfur batteries: an analytical study using the organic conversion technique

Cite this: DOI: 10.1039/xoxxoooooox

Received ooth January 2012,
Accepted ooth January 2012

DOI: 10.1039/xoxxoooooox

www.rsc.org/

Ayako Kawase*[a], Soichi Shirai[b], Yoshinari Yamoto[c], Ryuichi Arakawa[c] and Toshikazu Takata[d]

This investigation elucidates the electrochemical reaction process occurring within lithium-sulfur battery cells in detail, which have been unclear even after a half century of study primarily due to the very high reactivity of the polysulfide species. The polysulfide intermediates were deactivated by organic conversion – benzylization, and LC/MS and NMR analyses were first applied. The results demonstrate that the second voltage plateau in the discharge profile, which is the most important step in practical use because of its constant voltage, is dominated by the reduction of Li_2S_3 intermediate. The first voltage plateau and the transition state between the plateaus, in which the voltage varies with the capacity, are associated with multiple reactions including the decomposition of S_8 to Li_2S_x (x = 1 to 7) and the transformation of Li_2S_y (y = 4 to 8) to Li_2S_z (z = 1 to 3). It is also revealed that longer polysulfide species,Li_2S_i (i = 6 to 8) are responsible for redox shuttle phenomenon, which cause serious capacity degradation.

Introduction

The research and development of rechargeable batteries with sufficient energy storage is becoming one of the most active aspects of the automobile and the power industry, due to the rapidly increasing demands for environmentally-friendly electric vehicles and load leveling systems. One potential candidate for next-generation rechargeable batteries is the *lithium-sulfur battery*, which offers high theoretical specific capacity of 1680 mAh/g in addition to a specific energy value of 2570 Wh/kg. Its capacity is more than six times that of lithium ion batteries based on $LiCoO_2$.[1] Lithium-sulfur battery technology is also attractive since sulfur is a plentiful natural resource and thus is low in cost. Compared to the lithium-air cell, lithium-sulfur batteries can be compactly packaged and thus can be used to replace currently-used lithium ion battery systems with less difficulty. However, there are still challenges in practical applications of lithium-sulfur batteries such as low sulfur utilization due to sulfur's insulating properties and capacity degradation resulting from dissolution-deposition cycling or redox shuttle phenomenon.[2] Additional insights into the electrochemical reactions within a lithium-sulfur cell are of critical importance with regard to mitigating these shortcomings.

The polysulfide compounds generated in a lithium-sulfur cell have been intensively studied over a half century[3-5] because identification of the reactants, intermediates and products in the cell is a fundamental step in understanding the electrochemical reactions. The following reaction scheme has been suggested by ultraviolet-visible absorption (UV-vis) spectroscopic studies.[3]

$$S_8 + 2e^- \rightarrow S_8^{2-} \quad (1)$$
$$S_8^{2-} + 2e^- \rightarrow 2S_4^{2-} \quad (2)$$
$$S_8^{2-} \rightleftarrows S_6^{2-} + \tfrac{1}{4}S_8 \quad (3)$$
$$S_6^{2-} \rightleftarrows 2S_3^{-} \quad (4)$$

The details of these reactions are still unclear, however, because the UV-Vis absorption bands of some polysulfide molecules including unidentified species may overlap. The absence of reference spectra for isolated polysulfide compounds further complicates the situation. Equations 5 through 8 with Equations 1 and 2 are also widely accepted.[1,6]

$$3S_8^{2-} + 2e^- \rightarrow 4S_6^{2-} \quad (5)$$
$$2S_6^{2-} + 2e^- \rightarrow 3S_4^{2-} \quad (6)$$
$$S_4^{2-} + 2e^- \rightarrow 2S_2^{2-} \quad (7)$$
$$S_2^{2-} + 2e^- \rightarrow 2S^{2-} \quad (8)$$

These equations are based on the hypothesis that the eight-membered ring sulfur is reduced with respect to an even number of sulfur atoms. However, the hypothesis has not been authenticated by experimental studies.

In-situ measurements of reactions within a cell are associated with difficulties since some polysulfide molecules readily transform in solution. IR and Raman spectroscopic studies have been performed, but these analyses have faced difficulties in peak assignments as well as UV-Vis.[4] In particular, IR and Raman peak assignments for polysulfide species larger than S_4^{2-} have rarely been reported. Although, in principle, the number of sulfur atoms in a polysulfide molecule can be determined by mass spectrometry (MS), some polysulfide molecules transform even during the injection and ionization due to their high reactivity. The sensitivity of ^{33}S nuclear magnetic resonance spectrometry (NMR) is insufficient for elucidation of the structures of polysulfide molecules. Thus, ingenious methods of analysis are required to overcome these

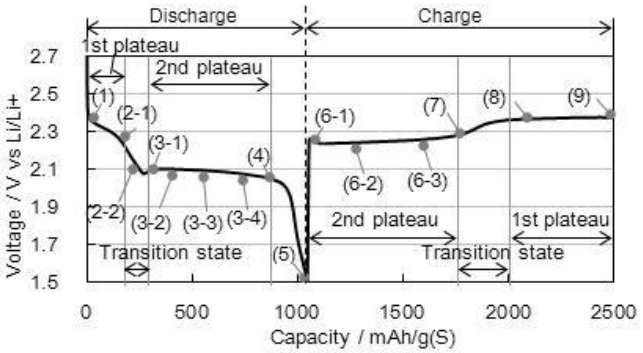

Fig. 1: Lithium-sulfur cell discharge-charge profile. Discharge-charge profile of lithium-sulfur cell during the first cycle with observation points.

shortcomings and to obtain additional insights into the detailed reaction mechanism.

It has recently been reported that sodium polysulfide species (Na_2S_x) can be converted to benzylized polysulfide (Bz_2S_x) molecules without changing the number of S atoms. The Bz_2S_x species can be analyzed via proton NMR (^{1}H NMR).[7] This organic conversion technique can be also applied to lithium polysulfide (Li_2S_x) species and therefore enable us to follow electrochemical reactions in battery cells using ^{1}H NMR. Furthermore, liquid chromatography-mass spectrometry (LC/MS) become also applicable, since the benzylized polysulfide species are sufficiently stable in the LC/MS environment.[8] Since, to the best of our knowledge, ^{1}H NMR spectra of isolated benzylized polysulfide species are rarely available, we instead utilize *ab initio* molecular orbital (MO) calculations for peak assignments. Ab initio MO calculations can be also useful in peak assignment and interpretation of ambiguous UV-Vis spectra.[9]

In this study, the polysulfide species within a lithium-sulfur cell have been identified utilizing LC/MS and NMR following application of the organic conversion technique, in order to elucidate the electrochemical reactions in more detail. UV-Vis spectra were also obtained to confirm consistency of the results of this work with those of previous studies.

Results and discussion

LC/MS Analysis

The charge-discharge profile of the lithium-sulfur cell during first cycle, showing the specific measurement points, is presented as Fig. 1. Distinctive plateaus appear at approximately 2.3 and 2.1 V, and the slope between 2.3 and 2.1 V can be regarded as the transition state. It is notable that the voltage varies with the capacity in the first plateau and the transition state, while the voltage is almost constant in the second plateau.

The LC data associated with the discharge process are shown in Fig. 2(a), along with reference data for Bz_2S, Bz_2S_2 and S_8. LC peaks for Bz_2S_x were successfully identified by MS (see Supporting Information, Fig. S1), and peak for S_8 was identified by reference. The amount of each species relative to its original concentration at each point is estimated from the peak area and summarized in Table 1. The amount change of Bz_2S_x (x = 1 to 6) is shown in Fig. 2(b).

It is evident that the concentration of S_8 decreases between points 1 and 3-2, and that all possible species produced by the decomposition of S_8, including Li_2S_7, Li_2S_5, Li_2S_3, Li_2S_2 and Li_2S are detected at point 2-1. These species were undetected in previous studies.[4-6] Li_2S_5, Li_2S_4 and Li_2S_3 are major, while Li_2S_8 is minor. The increasing rate of Li_2S_x (x = 4 to 8) species makes a downward turn between points 2-1 and 3-1, and these species completely disappear at point 3-3. Li_2S_3, which is dominant at point 3-2, gradually decreases up to point 4, and Li_2S and Li_2S_2 increase over this same span. Beginning at point 3-4, Li_2S increases at an accelerated rate, while the increasing rate of Li_2S_2 is reduced.

Table 1. LC peak identification by MS and the relative remaining quantity of species as estimated from LC data.

		S_8	Li_2S_8	Li_2S_7	Li_2S_6	Li_2S_5	Li_2S_4	Li_2S_3	Li_2S_2	Li_2S
m/z $[Bz_2S_x+NH_4]^+$		-	456	424	392	360	328	296	264	-
Retention time /min.		12.6	25.2	18.6	14.0	10.6	8.0	6.5	5.1	4.6
Relative amount at observation points	1	184	0	0	0	0	0	0	0	0
	2-1	103	6	10	27	109	86	68	4	14
	2-2	32	6	11	33	135	112	97	8	8
	3-1	14	4	7	27	129	126	144	21	15
	3-2	4	1	3	15	80	116	242	101	25
	3-3	0	0	0	0	0	9	264	163	23
	3-4	0	0	0	0	0	8	100	392	29
	4	0	0	0	0	1	1	1	494	134
	5	0	0	0	0	0	0	2	348	489
	6-1	0	0	0	0	0	1	1	253	505
	6-2	0	0	0	0	2	1	0	328	171
	6-3	0	0	1	3	31	68	216	169	30
	7	2	1	2	11	73	104	231	61	20
	8	35	5	10	29	115	100	83	5	11

These results suggest that the overall electrochemical reaction can be divided into four major stages. The first stage is between points 1 and 3-1 (in the first plateau and the transition state). The second stage is between points 2-1 and 3-3 (in the transition state and the beginning of the second plateau). The third stage is from points 3-1 to 4 (in the second plateau). The fourth stage is from points 3-4 to 5 (in the latter half of the second plateau and after the plateau).

In the first stage, S_8 is either reduced to Li_2S_8 or smaller species directly, and this decomposition of S_8 likely continues up to point 3-1. The first stage (from point 1 to point 3-1) is described by Equations 9 through 13.

$$S_8 + 2e^- \rightarrow S_8^{2-} \quad (9)$$
$$S_8 + 4e^- \rightarrow S_7^{2-} + S^{2-} \quad (10)$$
$$S_8 + 4e^- \rightarrow S_6^{2-} + S_2^{2-} \quad (11)$$
$$S_8 + 4e^- \rightarrow S_5^{2-} + S_3^{2-} \quad (12)$$
$$S_8 + 4e^- \rightarrow 2S_4^{2-} \quad (13)$$

The increase in Li_2S_x (x = 1 to 3), concurrent decline of Li_2S_y (y = 4 to 8) and disappearance at point 3-3 suggest that the Li_2S_y (y = 4 to 8) is reduced to Li_2S_x (x = 1 to 3) in the second stage. The second stage (from point 2-1 to point 3-3) is denoted by Equations 14 through 20.

$$S_8^{2-} + 2e^- \rightarrow S_6^{2-} + S_2^{2-} \quad (14)$$
$$S_8^{2-} + 2e^- \rightarrow S_5^{2-} + S_3^{2-} \quad (15)$$
$$S_8^{2-} + 2e^- \rightarrow 2S_4^{2-} \quad (16)$$
$$S_7^{2-} + 2e^- \rightarrow S_4^{2-} + S_3^{2-} \quad (17)$$
$$S_6^{2-} + 2e^- \rightarrow 2S_3^{2-} \quad (18)$$
$$S_5^{2-} + 2e^- \rightarrow S_3^{2-} + S_2^{2-} \quad (19)$$
$$S_4^{2-} + 2e^- \rightarrow 2S_2^{2-} \quad (20)$$

The Li_2S_3 produced in the first and second stage is subsequently reduced to Li_2S_2 and Li_2S in the third stage. The third stage (from point 3-1 to point 4) is represented by Equation 21.

$$S_3^{2-} + 2e^- \rightarrow S_2^{2-} + S^{2-} \quad (21)$$

In the latter half of the second plateau and subsequent plateau, the Li_2S_2 is partly reduced to Li_2S in the fourth stage. The

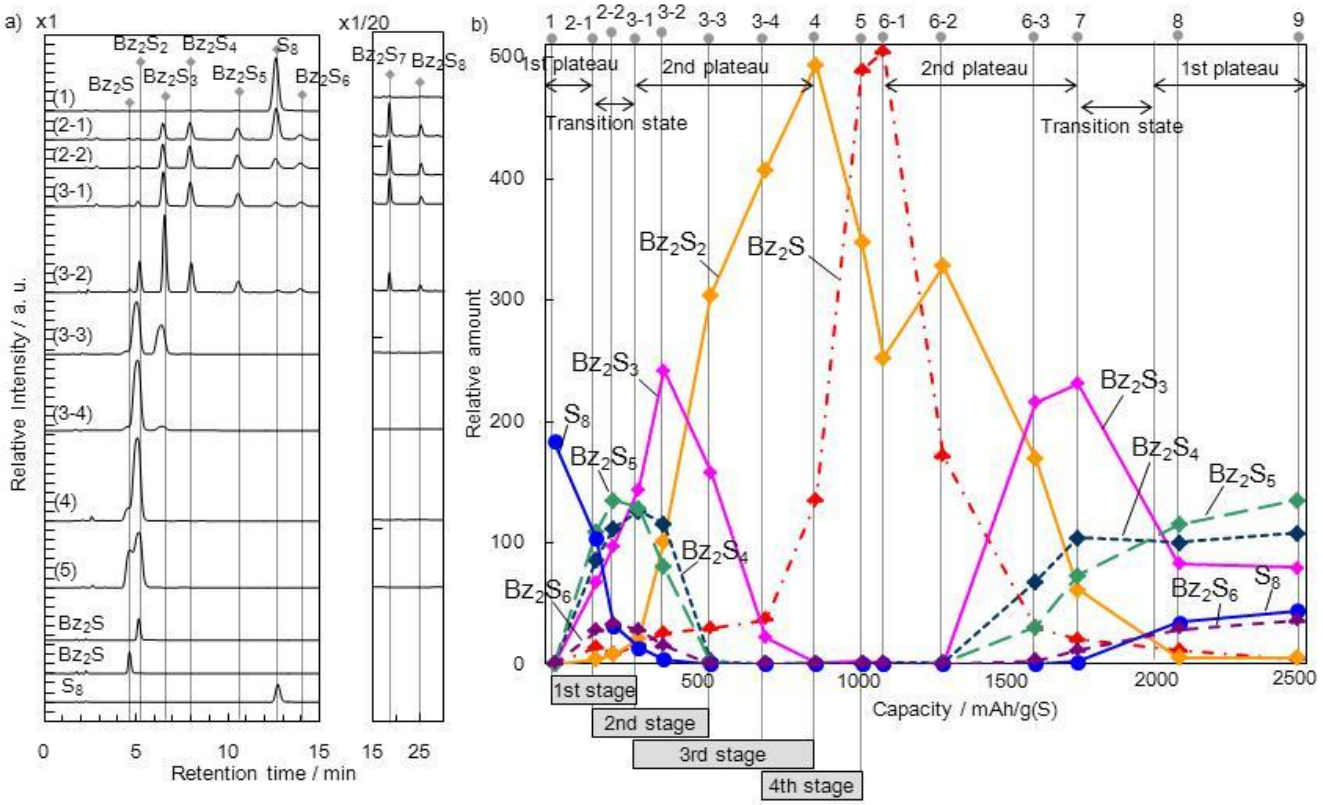

Fig. 2: LC/MS results at points during cell discharge-charge. (a) LC data for points 1 to 5, including Bz_2S, Bz_2S_2 and S_8 as references. (b) Relative remaining quantity of Bz_2S_x (x = 1 to 6) at points 1 to 9 as estimated from LC data.

fourth stage does not complete, judging from the observation that most of the Li_2S_2 remains intact. The fourth stage (from point 3-4 to point 5) is represented by Equation 22.

$$S_2^{2-} + 2e^- \rightarrow 2S^{2-} \quad (22)$$

It is worth noting that the second plateau with a constant voltage is associated with simple reaction – the reduction of Li_2S_3. On the other hand, in the first plateau and the transition state in which the voltage changes drastically, multiple reactions occur simultaneously. The quantities of polysulfide species in those regions in which multiple reactions overlap can be considered as the sum total generated by the simultaneous reactions.

Equations 9, 16, 20 and 22 correspond to the previously proposed reactions, which are shown above as Equations 1, 2, 7 and 8 respectively.[1,3,6] The other reactions are newly proposed in this study.

Reverse reactions occur in the charging process. It is evident, however, that Li_2S_x (x = 4 to 8) increase and Li_2S_3 keeps its amount from points 8 to 9. This phenomenon is attributed to the redox shuttle phenomenon, in which the polysulfide migrate onto the Li anode and reduced on the spot, resulting in the endless charge of such cells.[2] The shuttle phenomenon occurs between points 8 and 9 (in the first plateau in charging process), in which longer Li_2S_y (y = 6 to 8) appear. The results suggest that longer Li_2S_y (y = 6 to 8) are responsible for shuttle phenomenon, and they are reduced to shorter Li_2S_z (z = 3 to 5) on the Li anode. The shuttle phenomenon can be suppressed by electrolyte additives or protection layers of Li anode.[2]

NMR Analysis

The ^{1}H NMR spectra of benzylized polysulfide species in the electrolyte solutions are shown in Fig. 3(a), along with spectra for Bz_2S and Bz_2S_2 as reference. The peaks, which appear in the region from 3 to 5 ppm, correspond to methylene H of the benzylized polysulfides. The peak at 3.60 ppm, which can be assigned to either Bz_2S or Bz_2S_2, is the most prominent at point 5 and is observed at all points except point 1. Three major peaks at 4.02, 4.15 and 4.20 ppm can be assigned to Bz_2S_x (x = 3, 4, 5) according to the LC/MS results. The calculated relative chemical shifts for Bz_2S_y (y = 3 to 8) summarized in Fig. 3(a) suggest the following peak assignments: 4.02 ppm to Bz_2S_3, 4.15 ppm to Bz_2S_4, and 4.20 ppm to Bz_2S_5.

The relative concentrations of the species estimated from peak areas are shown in Fig. 3(b). These results demonstrate that Li_2S_5, Li_2S_4, Li_2S_3, along with small amounts of Li_2S_2 and/or Li_2S, were generated between points 1 and 2-1, and that both Li_2S_5 and Li_2S_4 have disappeared by point 3-4. Li_2S_3 is the dominant species at point 3-2 and then fragments into Li_2S_2 and/or Li_2S from point 3-1 to point 5. These findings are qualitatively consistent with the LC/MS results.

In the case of Bz_2S_x (x = 1 to 5), the calculated chemical shift increases with the number of S atoms, as a result of withdrawal of the electrons from benzyl group by the polysulfur moieties (due to the high electronegativity of S). The electron withdrawing strength of the polysulfur moiety increases with increasing number of S atoms because the negative charge can be more widely distributed and hence stabilized throughout the expanded orbitals. Conversely, however, the chemical shift decreases in the order of $Bz_2S_5 > Bz_2S_6 > Bz_2S_7 > Bz_2S_8$. In the optimized Bz_2S_5 geometry, one of the methylene H is located

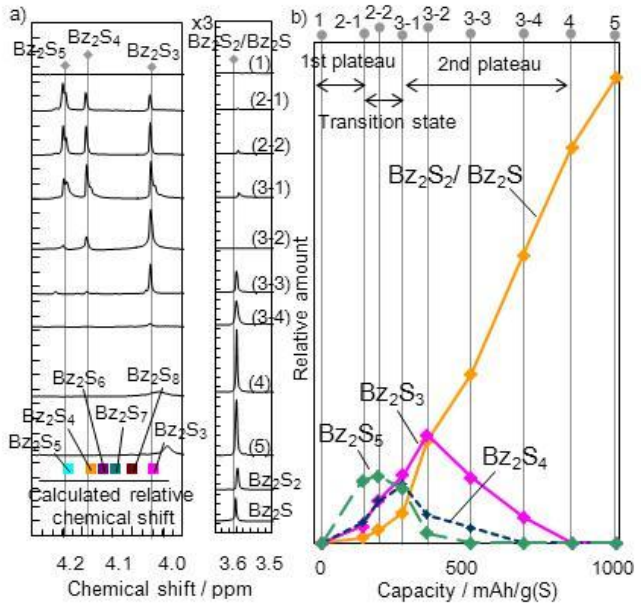

Fig. 3: ^{1}H NMR results at points during cell discharge.(a) ^{1}H NMR spectra at chemical shift for points 1 to 5, along with data for Bz_2S, Bz_2S_2 and calculated relative chemical shifts for Bz_2S_x (x = 3 to 8) as references. (b) Relative remaining quantity of species as estimated from ^{1}H NMR spectra.

close to the fifth S atom, resulting in a H bonding-type interaction (see Supporting Information, Fig. S3). It has been shown that the chemical shift of the H closest to the S atom in Bz_2S_5 is remarkably high because of the deshielding by S atoms with the electron withdrawing property. In the case of Bz_2S_x (x = 6 to 8), the methylene H is further removed from the sulfur atom, resulting in the lower chemical shift.

UV-Vis Analysis

The UV-Vis spectra of the electrolytes in the cell are shown in Fig. 4(a). No peaks are observed in the region above 300 nm at point 1, whereas a peak appears at 430 nm at point 2-1, and a prominent peak at 400 nm along with a smaller peak at 610 nm are both observed at point 3-1. Both the 400 and 610 nm peaks gradually decrease during the second plateau (from points 3-1 to 5). In the charging process, reverse reactions are observed except for point 9 (see Supporting Information, Fig. S4), as well as LC/MS results. The simulated UV-Vis spectra incorporating the solvent effect of dimethoxyethane (DME) are shown in Figs. 4(b) to (g). The simulated spectra indicate that some of the Li_2S_x species produce characteristic peaks in the region above 300 nm; both Li_2S_8 and Li_2S_7 have absorption bands at 430 nm and Li_2S_6 has a band at 400 nm. Most radical species show significantly red-shifted peaks, and the LiS_3 radical has a peak at 610 nm. These calculated results suggest that Li_2S_8 and/or Li_2S_7 are produced at point 2-1 and Li_2S_6 and the LiS_3 radical is generated at point 3-1. The large absorption band which appears between 300 and 400 nm can be assigned to a mixture of Li_2S_x (x = 1 to 8) species and/or radicals. The results of the analysis are consistent with LC/MS and NMR results.

The absorption wavelengths obtained in both experimental and calculated results incorporating the solvent effects of DME and dimethylformamide (DMF) are compared in Table 2. This comparison shows that the calculation results are largely consistent with both present and previous experimental results.

Table 2. Experimental and calculated UV-Vis absorption wavelengths for Li_2S_8 Li_2S_6 and LiS_3 in DME and DMF.

Solvent	Method	Absorption bands / nm		
		Li_2S_8	Li_2S_6	LiS_3 radical
DME	Experiment	430	400	610
	Calculation	453	413	613
DMF	Experiment[5]	505	460	618
	Calculation	492	436	648

The calculation results suggest that the reaction products Li_2S_7, Li_2S_5 and Li_2S_3 have gone undetected in prior studies, since their absorption bands overlap one another. Thus, these species are hardly determined by conventional UV-Vis.

A detailed analysis of the calculation results reveals that the absorbance of Li_2S_x species above 300 nm results from HOMO-LUMO single electron transitions. The HOMO and LUMO energies in Li_2S_x are compared in Supporting Table S1. In the larger Li_2S_x (x = 4 to 8), the HOMOs are mainly distributed to those S atoms which are close to Li atoms and the LUMOs distribute around the centers of the molecules as shown in Fig. 4(h). Therefore, the HOMO-LUMO transition can be regarded as an intramolecular charge transfer from the edges to the center of the molecule. The HOMOs mainly consist of S 3p orbitals and the LUMOs consist of S 4s and/or 4p orbitals. The HOMO-LUMO transition energy decreases with the number of S atoms since the LUMO can be stabilized by S atoms as a result of their high electronegativity. In contrast, the HOMOs are destabilized by Li atoms, due to their strong electron-donating abilities. The absorptions of the radical species can be attributed to the transition from β–HOMO to β–LUMO. A very small energy gap between β–HOMO and β–LUMO is responsible for the long absorption wavelength.

The LUMO of S_8 distribute uniformly to each S atom. This result supports the LC/MS result that S_8 is reduced to all possible species produced by the decomposition of S_8 including Li_2S_7, Li_2S_5, Li_2S_3 and Li_2S, because all bonds of S_8 can be split by delocalized LUMO. The theoretical result that LUMOs are localized around the centers of the Li_2S_x (x = 4 to 8) molecules supports the experimental result that the Li_2S_x (x = 4 to 8) are split around the centers of the molecules.

Experimental

Experimental details

Cathodes were composed of 60 wt% sulfur, 30 wt% carbon (Ketjenblack EC-600 JD), 8 wt% polytetrafluoroethylene binder and 2 wt% carboxymethylcellulose thickener. A slurry made from these cathode materials mixed with water was applied to etched Al foil and then dried, after which the cathode sheets were cut into disks (φ = 10 mm) and pressed. The finished sulfur cathodes (80 μm thickness, 8 g/cm^2) were assembled in coin-type cells (CR2032) along with polyethylene separators (S6722, Asahi Kasei), Li foil (150 μm thickness) and electrolyte solutions (60 μl) consisting of 1.5 M lithium bis(trifluoromethanesulfonyl) imide in DME and dioxolane. The discharge-charge profiles were obtained using a current density of 0.8 mA cm^{-2} and voltages between 1.5 and 2.7 V at 25 °C.

All the subsequent sample preparation procedures were conducted under an Ar atmosphere. During the discharge-charge reaction, the cathodes were removed from the cells at various points within the process. The cathode, still wet with

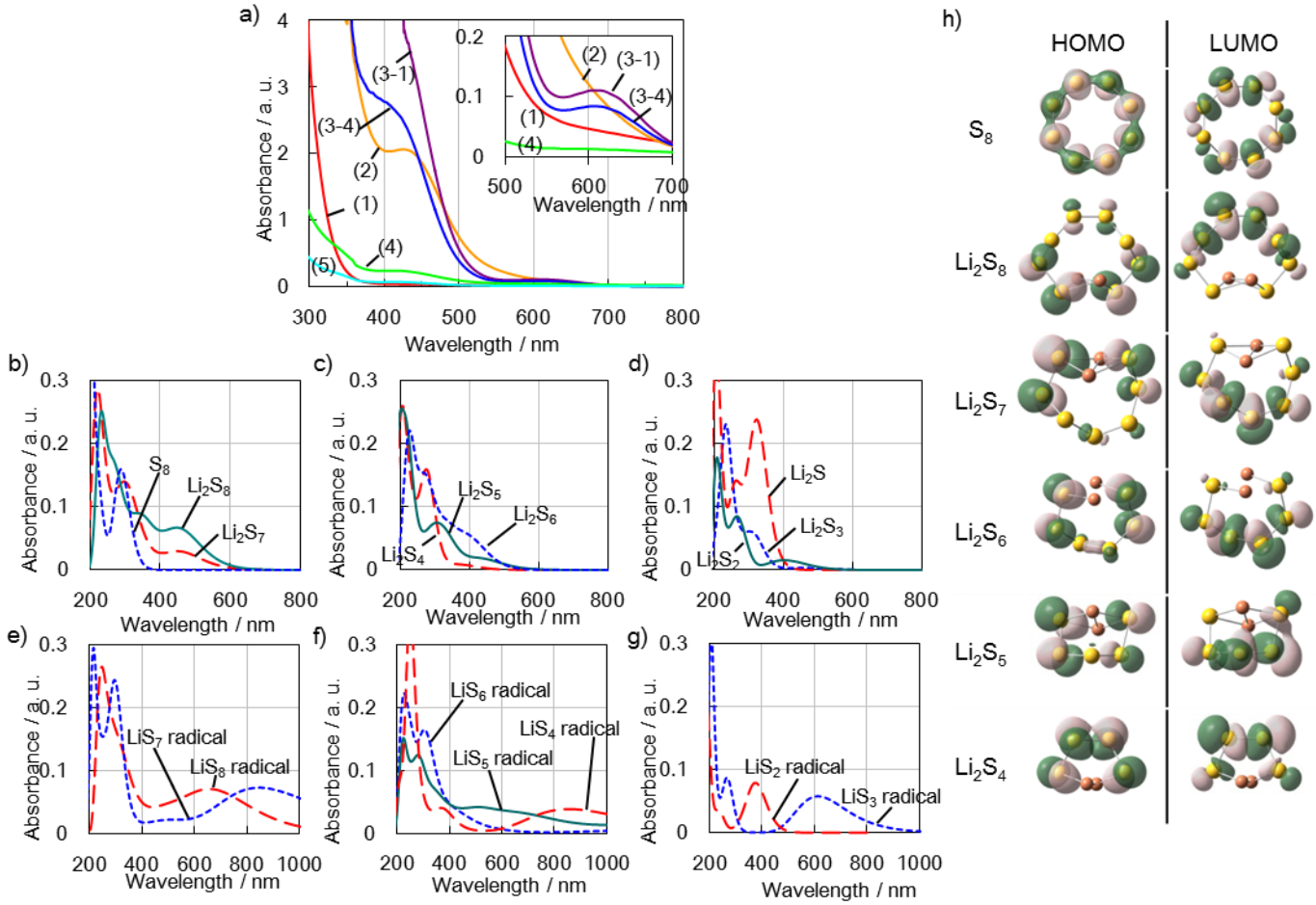

Fig. 4: Experimental and calculated UV-Vis spectra. a) Experimental UV-Vis spectra of electrolyte solutions over the discharge process. Calculated spectra with DME solvent effect for: b) S_8, Li_2S_8 and Li_2S_7; c) Li_2S_6, Li_2S_5 and Li_2S_4; d) Li_2S_3, Li_2S_2 and Li_2S; e) LiS_8 and LiS_7 radicals; f) LiS_6, LiS_5 and LiS_4 radicals; and g) LiS_3 and LiS_2 radicals. h) HOMO and LUMO visualizations based on model calculations for lithium-polysulfide and sulfur (yellow, S; and red, Li).

electrolytes, was immersed in l ml of DME and the resulting solution was transferred into a 1 mm path length quartz cell and examined by UV-Vis spectroscopy using a Shimadzu UV-3100PC.

For LC/MS and ^{1}H NMR measurements, cathodes taken from cells in the same manner were instead immersed in a mixture of DME and benzyl chloride, after which the cathode was pulverized by ultrasonication. Each sample was then allowed to sit for three hours to convert the lithium polysulfide (Li_2S_x) to benzylized polysulfide (Bz_2S_x).The conversion of Li_2S_x (x = 3 to 8) is almost complete with in three hours (see Supporting information, Fig. S6 and Fig. S7). On the other hand, three-hour conversion is supposed to be insufficient for Li_2S_x (x = 1 to 2) because of those pour solubility. Therefore, the half of each sample was allowed to sit for four days to get the highest conversion rate for Li_2S (see Supporting information, Fig. S8). The conversion ratio of Li_2S_x (x = 1 to 2) is supposed to be higher than 66%. Though the chain length of Bz_2S_x (x = 6 to 8) can be shortened during the long-time conversion, obtained Bz_2S_x (x = 3 to 8) by three-hour conversion should reflect the relative amounts of Li_2S_x in cathodes (see Supporting information, Fig. S7). S_8 dissolved in the solution remain unreacted during the time. The residual carbon matrix and current collector were subsequently removed by filtration, after which the solvent was evaporated. Sulfur and Bz_2S_x were dissolved in either tetrahydrofuran (THF) or deuterated chloroform. Sulfur and Bz_2S_x samples that were dissolved in THF were analyzed via LC/MS, and the samples that were dissolved in deuterated chloroform were analyzed using ^{1}H NMR. LC/MS experiments were carried out on a Thermo Scientific Exactive mass spectrometer, equipped with an atmospheric pressure chemical ionization (APCI) source, and interfaced to a Dionex Ultimate 3000 LC system with a 254 nm UV detector. Samples were first diluted with methanol and then injected onto an Intersil ODS-3 (150 x 2.1 mm, 5 µm) column, using a mobile phase composed of 10% aqueous ammonium acetate (5 mM) and 90% methanol at a constant flow rate of 200 µL/min. MS data were collected in positive ion mode as the ammonium adduct. To allow quantitative analysis, LC peak area for S_8, Bz_2S and Bz_2S_2 were converted to a relative analyte amount using calibration curves derived from standard solutions, and peak area for Bz_2S_x (x = 3 to 8) were converted based on the calculated relative absorbance at 254 nm. NMR data were recorded on a JEOL AL-400 spectrometer.

Computational details

Lithium-polysulfide molecules, which can be generated in the electrochemical reactions within the lithium-sulfur cell, were prepared. The closed-shell species were S_8, Li_2S_8, Li_2S_7, Li_2S_6, Li_2S_5, Li_2S_4, Li_2S_3, Li_2S_2 and Li_2S, while the open-shell radical

species were LiS_8, LiS_7, LiS_6, LiS_5, LiS_4, LiS_3 and LiS_2. Bz_2S_x models were prepared by replacing the Li atoms in these species with a benzyl group ($C_6H_5CH_2$-).

The molecular geometries were first optimized using density function theory (DFT) calculations. The ^{1}H NMR chemical shifts for Bz_2S_x were calculated using DFT combined with the gauge-independent atomic orbital (GIAO) technique.[10] The shielding constant of tetramethylsilane (TMS) was calculated to be 31.7947 ppm using the same theoretical approach and this was employed as the standard. The calculated chemical shifts for the four methylene H were represented by the average of their individual values. The excited states of polysulfide compounds were calculated using time dependent DFT (TD-DFT) calculations[11] in order to simulate their UV-Vis spectra, and each peak was represented by a Gaussian function with a maximum height proportional to the oscillator strength, using a full width at half maximum (FWHM) value of 0.73 eV. The solvent effect of methanol, DME and DMF on UV-Vis spectra were accounted for by utilizing a polarizable continuum model with the integral equation formalism variant (IEFPCM). The B3LYP exchange-correlation functional[12] was utilized for both DFT and TD-DFT and the 6-311+G (2d,p)[13] basis sets were employed for the calculation of ^{1}H NMR chemical shifts, while 6-31+G (d) for all other calculations.[14] All calculations were performed using the Gaussian03 program.[15]

Conclusions

The lithium polysulfide species generated in a lithium-sulfur cell were analyzed by LC/MS and NMR combined with organic conversion technique. The results suggested that electrochemical reactions in the cell proceed through four distinct stages. It is of particular interest that the second plateau in the discharge profile, which is the most important reaction state in practical use because of its constant voltage, is dominated by the reduction of Li_2S_3, while the first plateau and the transition state, in which the voltage varies with the capacity, is associated with multiple reactions. It also revealed that longer polysulfide, Li_2S_x (x = 6 to 8) are responsible for redox shuttle phenomenon, which cause serious capacity degradation. These new analytical method is also useful in study of sulfur based redox flow cells and catholyte cells, because dissolved polysulfide are used as an active material in such cells.[16] This work is the first step of understanding the influence of current density and electrolyte components on the reaction scheme, which is connected with cell performances. Therefore these understanding lead to enhancement in input-output capability, cell capacity, and discharge-charge cycle durability.

Acknowledgements

The authors are grateful to Dr. Yoonho Kim, Mr. Hirotoshi Fujikawa, Mr. Ichiro Fujimura, Mr. Akihisa Kuruma and Dr. Hirohisa Tanaka of Daihatsu Motor Co., Ltd., for their support and encouragement during this work.

Notes and references

[a] Daihatsu Motor Co., Ltd., R&D Division, Ryuo, Gamo, Shiga 520-2593, Japan

[b] Toyota Central R&D Laboratories, Inc., Inorganic Materials Division, Nagakute, Aichi 480-1192, Japan

[c] Department of Applied Chemistry, Faculty of Chemistry, Materials and Bioengineering, Kansai University, 3-3-35 Yamate-cho, Suita 564-8680, Japan

[d] Department of Organic and Polymeric Materials, Tokyo Institute of Technology, Ookayama, Meguro-ku, Tokyo 152-8550, Japan

Electronic Supplementary Information (ESI) available: [details of any supplementary information available should be included here]. See DOI: 10.1039/b000000x/

1 P. G. Bruce, S. A. Freunberger, L. J. Hardwick and J.-M. Tarascon, *Nature Material*, 2012, **11,** 19; X. Ji and L. F. Nazar, *J. Mater. Chem.*, 2010, **20,** 9821; Y. Yang, G. Zheng and Y. Cui, *Chem. Soc. Rev.*, 2013, **42**, 3018.

2 Y. V. Mikhaylik and J. R. Akridge, *J. Electrochem. Soc.*, 2004, **151 (11),** A1969; D. Aurbach, E. Pollak, R. Elazari, G. Salitra, C. S. Kelley and J. Affinito, *J. Electrochem. Soc.*, 2009, **156,** A694; Y. Mikhaylik, I. Kovalev, R. Schock, K. Kumaresan, J. Xu and J. Affinito *ECS Transactions*, 2010, **25,** 23.

3 J. Paris and V. Plichon, *Electrochem. Acta*,1981, **26,** 1823; T. Fujinaga, T. Kuwamoto, S. Okazaki and M. Hojo, *Bull. Chem. Soc. Jpn.*, 1980, **53,** 2851.

4 S. Tobishima, H. Yamamoto and M. Matsuda, *Electrochim. Acta*, 1997, **42,** 1019; R. J. H. Clark and D. G. Cobbold, *Inorg. Chem.*, 1978, **17,** 3169; T. Chivers and I. Drummond, *Inorg. Chem.*, 1972, **11,** 2525; T. Chivers and I. Drummond, *J. Chem. Soc.*, 1974, **(D),** 631.

5 W. F. Giggenbach, *J. Chem. Soc.*, 1973, **(D),** 729; F. Seel and H.-J. Guttler, *Angew. Chem. Int. Ed. Engl.*, 1973, **12,** 420; F. Seel, H.-J. Guttler, G. Simon and A. Wieckowski, *Pure & Appl. Chem.*, 1977, **49,** 45; J. Badoz-Lambling, R. Bonnaterre, G. Cauquis, M. Delaamar and G. Demange, *Electrochim. Acta*, 1976, **21,** 119; M. V. Merritt and D. T. Sawyer, *Inorg. Chem.*, 1970, **9,** 211; R. P. Martin, W. H. Doub, J. L. Roberts Jr. and D. T. Sawyer, *Inorg. Chem.*, 1973, **12,** 1921; M. Delamar and J.-C. Marchon, *J. Electroanal. Chem.*, 1975, **63,** 351; M. Delamar, *J. Electroanal. Chem.*, 1975, **63,** 339; R. D. Rauh, F. S. Shuker, J. M. Marston and S. B. Brummer, *Inorg. Nucl. Chem.*, 1977, **39,** 1761; K. M. Abraham, R. D. Rauh and S. B. Brummer, *Electrochim. Acta*, 1978, **23,** 501; J. C. Dobson, F. R. McLarnon and E. J. Cairns, *J. Electrochem. Soc.*, 1986, **133,** 1549; J. C. Dobson, F. R. McLarnon and E. J. Cairns, *J. Electrochem. Soc.*, 1986, **133,** 2069; P. Lessner, J. Winnick, F. R. McLarnon and E. J. Cairns, *J. Electrochem. Soc.*, 1986, **133,** 2510; P. Lessner, J. Winnick, F. R. McLarnon and E. J. Cairns, *J. Electrochem. Soc.*, 1986, **133,** 2517; P. Lessner, J. Winnick, F. R. McLarnon and E. J. Cairns, *J. Electrochem. Soc.*, 1987, **134,** 2669; P. T. Cunningham, S. A. Johnson and E. J. Cairns, *J. Electrochem. Soc.*, 1972, **119,** 1448.

6 K. Kumaresan, Y. Mikhaylik and R. E. White, *J. Electrochem. Soc.*, 2008, **155,** A576.

7 N. Yamada, M. Furukawa, M. Nishi and T. Takata, *Chem. Lett.*, 2002, **31,** 454; T. Takata, D. Saeki, Y. Makita, N. Yamada and N. Kihara, *Inorg. chem.*, 2003, **42,** 3712.

8 Y.W. Park, Y. Na and D.-J. Baek, *Bull. Korean Chem. Soc.*, 2006, **27,** 2023.

9 J. A. Tossell, *Geochem. Trans.*, 2003, **4,** 28.

10 F. London, *J. Phys. Radium*, 1937, **8,** 397; R. McWeeny, *Phys. Rev.*, 1962, **126,** 1028; R. Ditchfield, *Mol. Phys.*, 1974, **27,** 789; K.

Wolinski, J. F. Hinton and P. Pulay, *J. Am. Chem. Soc.*, 1990, **112,** 8251; J. R. Cheeseman, G. W. Trucks, T. A. Keith and M. J. Frisch, *J. Chem. Phys.*, 1996, **104,** 5497.

11 M. E. Casida. *Recent Advances In Density Functional Methods, Recent Advances In Computational Chemistry*, World Scientific, Singapore, 1995, 155.

12 A. D. Becke, *J. Chem. Phys.*, 1993, **98,** 5648; C. Lee, W. Yang and R. G. Parr, *Phys. Rev. B*, 1988, **37,** 785.

13 R. Krishnan, J. S. Binkley, R. Seeger and J. A. Pople, *J. Chem. Phys.*, 1980, **72,** 650; A. D. McLean and G. S. Chandler, *J. Chem. Phys.*, 1980, **72,** 5639.

14 W. J. Hehre, R. Ditchfield and J. A. Pople, *J. Chem. Phys.*, 1972, **56,** 2257; J. D. Dill and J.A. Pople, *J. Chem. Phys.*, 1975, **62,** 2921; M.M. Francl, W. J. Pietro, W. J. Hehre, J. S. Binkley, M. S. Gordon, D. J. DeFrees and J. A. Pople, *J. Chem. Phys.*, 1982, **77,** 3654.

15 M. J. Frisch, et al., *Gaussian 03, Revision E.01* (Gaussian Inc., Wallingford, CT, 2004).

16 R. Demir-Cakan, M. Morcrette, Gangulibabu, A. Guéguen, R. Dedryvère and J.-M. Tarascon *Energy Environ. Sci.*, 2013, **6,** 176; R. D. Rauh, K. M. Abraham, G. F. Pearson, J. K. Surprenant and S. B. Brummer, *J. Electrochem. Soc.*, 1979, **126,** 523.

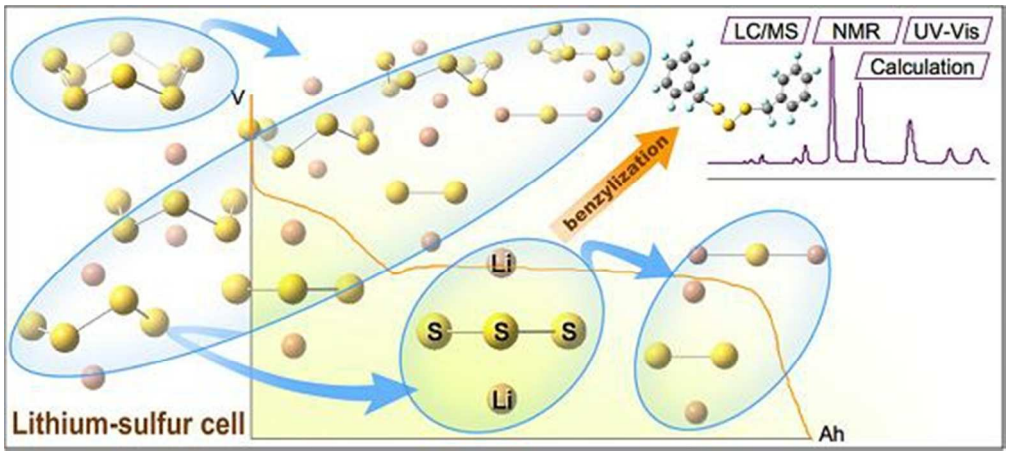

152x67mm (96 x 96 DPI)